

A Comprehensive Study of Sparse Representation Techniques for Offline Signature Verification

E. N. Zois, D. Tsourounis, I. Theodorakopoulos, A. L. Kesidis and G. Economou

Abstract— In this work, a feature extraction method for offline signature verification is presented that harnesses the power of sparse representation in order to deliver state-of-the-art verification performance in several signature datasets like CEDAR, MCYT-75, GPDS and UTSIG. Beyond the accuracy improvements, several major parameters associated with sparse representation; such as selected configuration, dictionary size, sparsity level and positivity priors are investigated. Besides, it is evinced that 2nd order statistics of the sparse codes is a powerful pooling function for the formation of the global signature descriptor. Also, a thorough evaluation of the effects of preprocessing is introduced by an automated algorithm in order to select the optimum thinning level. Finally, a segmentation strategy which employs a special form of spatial pyramid tailored to the problem of sparse representation is presented along with the enhancing of the produced descriptor on meaningful areas of the signature as emerged from the BRISK key-point detection mechanism. The obtained state-of-the-art results on the most challenging signature datasets provide a strong indication towards the benefits of learned features, even in writer dependent (WD) scenarios with a unique model for each writer and only a few available reference samples of him/her.

Index Terms— Off-line Signature Verification, Dictionary Learning, Sparse Coding, Spatial Pyramid, Feature Pooling, Image Preprocessing

1 INTRODUCTION

ONE of the most acceptable and long-standing behavioral modus to declare and verify a person's identity or acknowledge of his/hers consent in a wide variety of cases is the handwritten signature. Signatures are depicted by their trace, usually onto a sheet of paper or an electronic device. This process conveys information related not only to the imprinting of the personal details of the signatory, but also to his/her writing system and psychophysical state [1]. Ongoing research regarding the development of offline or static Automated Signature Verification Systems (ASV's/SV's) indicate clearly that this topic still is an active, open and important research field [2-6].

The purpose of an offline SV system is to recognize an image of a signature in question as genuine or forgery, i.e. to verify the writer's genuine signatures and reject the forgery ones. This work addresses writer dependent signature verification (WD) by employing a unique model for each participating writer with the use of some genuine reference samples and some genuine samples from other writers as representatives of the positive and negative class respectively.

Conceivably, the most influential step in the design of a SV system is the feature extraction stage, which can be defined as the process that maps any given signature image into a multidimensional vector. Feature extraction methods can be divided into two major categories: a) handcrafted features which aim at pre-determined characteristics of the image; examples of this branch include methods with global-local and/or grid-texture oriented features [7] and b) features learned directly from images,

where Deep Learning (DL) [2, 8-10], Bag of Visual Words (BoW) [11-13] or Histogram of Templates (HOT) [14] are some of the most representative techniques.

Learning features from images could potentially have significant advantages, since such techniques -in general- can discover specialized spatial associations that are inherent into the signature images. Among the most powerful categories of such methods is Sparse Representation (SR). At a glance, SR methods cope with the problem of signal representation. Frequently they involve an overcomplete basis or dictionary D which can be developed either by using a mathematical model or a set of data instances. The term "overcomplete" means that the population of the dictionary members (or atoms) is greater with respect to the dimensionality of one atom. Then, given a dictionary D along with an unknown signal X , SR handles the reconstruction, in an optimization context, of X by a linear combination of the atoms. The reconstruction is constrained by the fact that only as few as possible atoms are selected from the overcomplete dictionary for the minimization of the reconstruction error, something that promotes the sparsity of the representation. The benefit of having an over-complete basis is that the basis vectors can adapt to patterns inherent in the input data. Nevertheless, the use of an over-complete basis, may lead to coefficients which are no longer uniquely determined. Consequently, in SR, the additional criterion of sparsity is applied in order to resolve the degeneracy introduced by over-completeness. Figure 1, depicts the SR concept.

Sparse Representation techniques are the subject of

scientific interest for quite a long time [15-18] and have been proved to be extremely useful in computer vision and pattern recognition applications. This work presents for the first time a method for off-line signature verification that harnesses the power of SR in order to deliver state-of-the-art verification performance with the use of few genuine reference samples. The current paper introduces several advancements in the line of work initiated with two recently published papers investigating the potential of SR [19] and Archetypal Analysis (AA) [20] on the offline SV task. Beyond the accuracy improvements and the high-end performance achieved in several popular signature datasets, this work has a significant contribution towards the following directions:

1. We innovatively address several aspects of local feature pooling for offline SV. As a result, we provide evidence of the superiority of 2nd order statistics of the sparse coefficients as a powerful pooling function for the formation of the global signature descriptor. Combined with a segmentation strategy which employs a special form of spatial pyramid (SP) tailored to the problem of SV we provide a powerful feature extraction mechanism for SV.
2. We apply a standard mechanism for enhancing the verification efficiency of the produced descriptor on meaningful areas of the signature, by means of the key-point detection mechanism of BRISK descriptors.
3. We perform a thorough evaluation of the effects of preprocessing, especially thinning and introduce an automated algorithm to select the optimum thinning level in order to derive a signature's trace on the image plane.
4. We thoroughly investigate the impact of all the major parameters associated with SR, such as selected formulation (greedy approximation or convex relaxation), dictionary size, sparsity level etc. We also evaluate the effect to the overall performance of imposing additional priors into the corresponding optimization problems.

The paper is organized as follows: Section 2 provides a short literature review and summarizes the proposed approach. Section 3 discusses details of the signature preprocessing steps and highlights the feature formation process while Section 4 describes the utilized databases along with the evaluation protocol. Section 5 displays the corresponding experimental results. Finally, conclusions are drawn in Section 6. Appendices A and B provide elementary details regarding sparse representation and dictionary learning techniques while Appendices C and D provide two pseudocodes related to the present work.

2 LITERATURE REVIEW - SUMMARY OF THE METHOD

In accordance with Appendices A and B the following notations are introduced: A single patch is a column vector, defined as: $\mathbf{x}^i \in \mathbb{R}^{\text{SignalDim} \times 1}$ while matrices are formed by M -columns: $\mathbf{X} = [\mathbf{x}^1, \mathbf{x}^2, \dots, \mathbf{x}^M] \in \mathbb{R}^{\text{SignalDim} \times M}$. The K -atoms $\mathbf{d}^j \in \mathbb{R}^{\text{SignalDim} \times 1}$ of a dictionary are the columns of $\mathbf{D} = [\mathbf{d}^1, \mathbf{d}^2, \dots, \mathbf{d}^K] \in \mathbb{R}^{\text{SignalDim} \times K}$ matrix with $K > \text{signalDim}$ in order to express the overcomplete property. Finally,

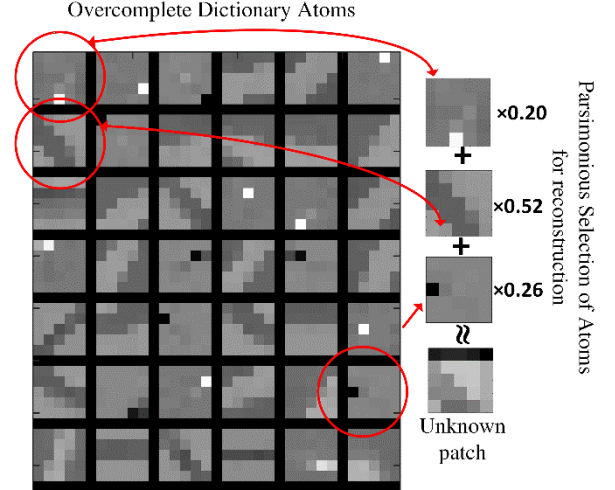


Fig. 1. Illustration of the SR concept. The dictionary is composed of forty-two atoms of 25 dimensions (5x5). For an unknown patch, a SR algorithm calculates new representation in the form of the sparsest linear combination of dictionary atoms that minimizes the reconstruction error.

the matrix $\mathbf{A} = [\mathbf{a}^1, \mathbf{a}^2, \dots, \mathbf{a}^M] \in \mathbb{R}^{K \times M}$ represents the sparse coefficients $\mathbf{a}^i \in \mathbb{R}^{K \times 1}$ for a single i -patch.

2.1. Related Work

A significant number of handcrafted feature extraction methods for offline signature verification rely on the evaluation of global and/or local signature descriptors as well as on grid-texture oriented features. With respect to the above family of feature descriptors, a diversity of feature extraction methods for offline SV has been proposed mainly for single-script [2-6] as well as for multi-script styles of signatures [21, 22]. Some other examples can be found in [19, 20] and their associated references. On the other hand, methods have been proposed that rely on learning features directly from the raw image data. Some efforts include the use of Restricted Boltzmann Machines (RBMs) in [23] and Convolutional Neural Networks (CNNs) [24, 25]. Soleimani et al. in [9] proposed the use of Deep Neural Networks for Multitask Metric Learning by employing a distance metric between pairs of signatures in which Local Binary Patterns is used as an intermediate feature vector. Rantzsch et al. [26] presented an approach named Signature Embedding which is based on deep metric learning. Specifically they compared triplets of two genuine and one forged signature, in order for their system to learn to embed signatures into a high-dimensional space. Following, they proposed a Euclidean distance metric as a means for measuring similarity. Hafemann et al. in a series of publications, proposed methods for learning features from images. Specifically, the authors in [27] introduced a formulation for learning features from genuine signatures by a development dataset, and used them in order to train writer dependent classifiers to another set of users. In [28] the authors obtained state-of-the-art results on several GPDS datasets using CNN architecture and in [29] they demonstrated a novel formulation that leverages knowledge of skilled forgeries for feature learning. In addition, the authors in [8] responded to the fixed size input constraint of the neural network by learning a

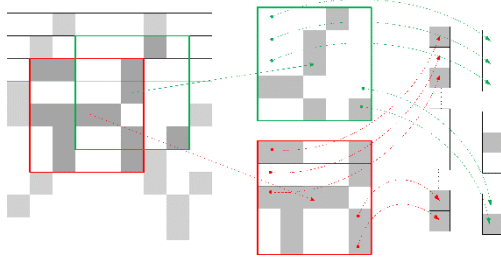


Fig. 2. Patch extraction detail. Left: The gray shades represent pixels of the trace of a signature. Center: Two patch windows of size 5 (5x5 pixels) centered or located at two different points of the signature trace. Right: The formation of the corresponding column-vectors by sequential column-wise concatenation of each patch's values.

fixed-sized representation from variable sized signature images with the integration of a spatial pyramid pooling layer.

Although SR methods have not been exploited for feature extraction in offline SV systems prior to [19, 20], in [30] a method for writer identification based on sparse representation of handwritten structural primitives, called graphemes or fraglets is presented. Similarly, in [31] an online signature verification technique appears based on discrete cosine transform (DCT) and sparse representation. In addition, some sort of codebook formation is also proposed in [32] by means of forming codebooks using signature samples of an independent database with the k-means algorithm and in [13] by creating a codebook of first order HOGs and then coding each feature to the nearest word in the codebook. Complementary, we were also motivated to pursue sparse coding and dictionary learning instead of k-means, since it has been stated that "whenever using k-means to get a dictionary, if you replace it with sparse coding it'll often work better" [33]. Therefore our intuition to use SR just got stronger.

2.2 Method Overview

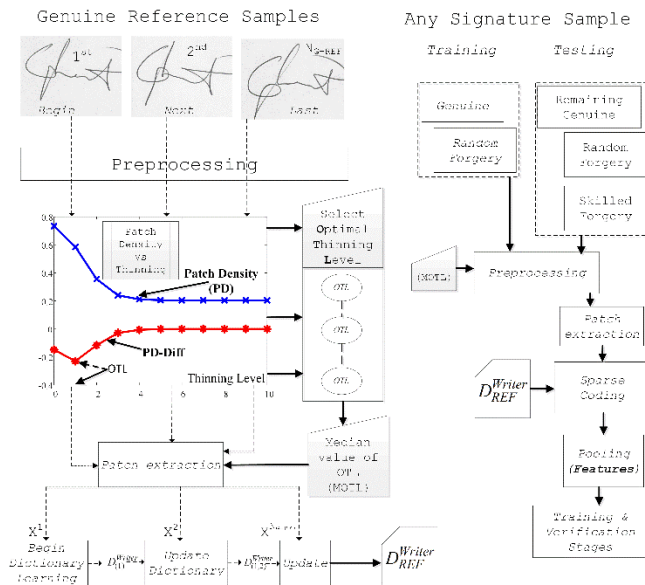


Fig. 3. A diagram of the proposed pipeline emphasizing the preprocessing and dictionary learning stages. The Optimal Thinning Level (OTL) at the preprocessing stage is selected from the extreme point of the patch density slope (located at the upper center of the Figure).

The proposed handwritten signature verification system utilizes a sparse representation framework in order to learn local features and construct a global signature descriptor. The two main approximations of sparse coding (greedy and convex relaxation) and their efficiency are thoroughly investigated. Various styles of pooling strategies including a novel, second order pooling function are also presented. In addition, a widespread key-point selection algorithm is also employed in order to further emphasize salient locations across the signature.

The preprocessing stage of grayscale signature images is kept as simple as possible given the fact that usually the signatures under examination have already undergone a noise - artefacts removal process. The major steps are: a) thresholding, followed by b) the morphological process of thinning. The Optimal Thinning Level (OTL) of each signature is defined with the use of its local patches, derived from the binary/thinned images. Specifically, patches are extracted from every pixel of the thinned signature's trace (i.e. by dense sampling, as shown in Figure 2) whereas the percentage of the signature pixels that inhabit each patch is also counted. This information helps us to define the patch density (PD) of a signature and plot it as a function of the number of successive thinning operations applied. In this way, the individual optimal thinning level (OTL) for each signature can be defined by utilizing the minimum value of its corresponding PD slope. Subsequently, the optimal thinning level (MOTL) for the reference samples of a writer is defined by their median value. The MOTL value is used for preprocessing of all the signature images that belong to the writer under consideration.

For SR, all the densely sampled patches $\{x^i\}$ of the signature trace are extracted from the grayscale signature image, at every i -position indexed by the skeleton pixels of the signature, obtained via the thinning process. Subsequently, the gray values of the patches associated with the genuine reference samples are transformed into column vectors and used as input $\mathbf{X} = \{x^i\}$ to a dictionary learning algorithm which evaluates the dictionary \mathbf{D} . Following, for every other signature, the patches are encoded, by means of evaluating the sparse coefficients $\mathbf{A} = \{a^i\}$ using the dictionary \mathbf{D} of the writer under consideration. The final feature of each signature image is formed by applying a pooling function $F(\mathbf{A})$ on the sparse vectors, using a specially designed spatial pyramid, which segments the signature skeleton in equimass parts. Additionally, the key-points derived from the BRISK [34] algorithm pinpoint image regions of interest, whereas the sparse codes of the corresponding nearby patches are also pooled together. The obtained pooled vector is concatenated with the spatial pyramid vector in order to form the final signature descriptor. The signature verification system is realized by a binary radial basis SVM classifier with the above features as inputs. The learning stage (i.e. training and validation) of the verifier, utilizes the positive class features derived from the genuine reference signatures as well as the negative class features derived from randomly selected genuine signatures from a subset of the remaining writers of the dataset. Figure 3 presents

a motif of the proposed system with emphasis on the preprocessing and the dictionary learning stages. The corresponding pseudocode is provided in Appendix C.

3. FEATURE EXTRACTION

3.1. Preprocessing

Preprocessing consists of two steps: binarization followed by thinning. The grayscale images are binarized using Otsu's method [35]. Then, successive morphological thinning operations are applied on the binary image in order to provide a gradual skeletonization of the signature. Intuitively, the outcome of the thinning operation affects the verification performance since it modifies the shape of the signature image. It has been experimentally observed [7] that the thinning level is critical for a Signature Verification (SV) system's performance and its optimal value is not the same for all databases. This work proposes a novel method for selecting the optimal thinning level (OTL) for each signature and consequently for each writer. As mentioned in Section 2.2, the OTL is defined as the number of thinning operations that results to the steepest descend of the density function. Following the enrollment of a set of genuine reference signatures for a person, its median value of the associated OTL values (MOTL) accompanies the design of each writer's model, i.e. $MOTL(N_{G-REF}) = \text{median}(OTL(i))$, where $i \in [1, \dots, N_{G-REF}]$. Hence, for any input signature which claims an identity, the number of thinning operations will be determined by the MOTL value of the signing person. Appendix D presents the proposed thinning procedure in an algorithmic form. Figure 4 presents the corresponding plots of the patch density, the patch density derivative, expressed by its associated patch density difference and OTL-MOTL values for one writer and an indicative number of his/hers genuine samples derived from all the signature datasets, namely CEDAR, MCYT-75, GPDS300 and UTSIG.

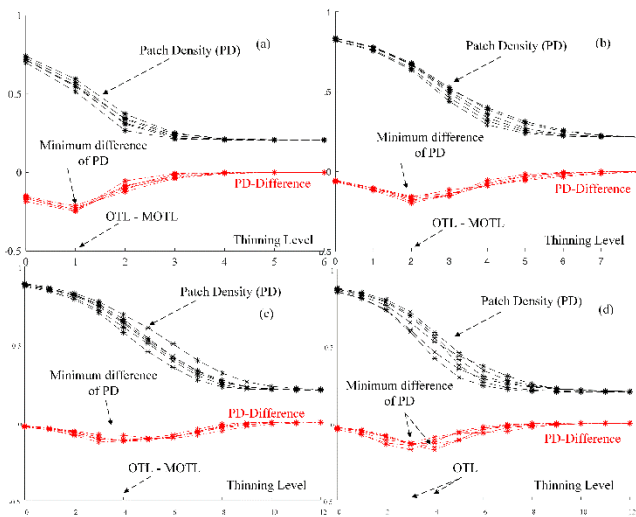


Fig. 4. Plots of the patch density (PD) and corresponding differences as a function of the thinning level. The above plots refer to one writer and an indicative set of six genuine samples derived from the (a) CEDAR, (b) MCYT-75, (c) GPDS300 and (d) UTSIG signature datasets, respectively. The patch size is set to 5.

The extracted results indicate that the genuine signatures that are part of the CEDAR dataset have the majority (~95%) of their OTL values to be equal to one with few (~5%) signature samples having their OTL values to two. For the MCYT-75 dataset the majority of their OTL values are equal to two with very few samples having their OTL values to three and four. For the GPDS300 dataset, the OTL values appear to distribute between 2 and 6, with an observed mode of 4, while for the UTSIG dataset OTL is equally distributed among values 2 and 3. Especially for the CEDAR and MCYT-75 datasets, Figure 4 indicates that they are more stable in terms of acquisition conditions comparing to datasets GPDS300 and UTSIG. Thus one could consider the SV problem addressed by CEDAR and MCYT-75 dataset to resemble a case study in which the aspect ratio and acquisition conditions do not vary significantly, similar to situations encountered in mobile financial applications.

3.2. Patch Extraction

The signature patches are extracted from the original grayscale signature image, indexed by the signature's skeleton pixels after applying the thinning operation MOTL times, as shown in Figure 4. Specifically, the patches' centers are sampled densely at every pixel of a signature's skeleton. As a consequence, the number of image patches equals the number of pixels of the signature's skeleton. Furthermore, the patches are centered, i.e. have their average intensity been subtracted in order to have a zero mean value. The centering of each patch produces data invariant to the mean intensity and the learned structures, like edges, are anticipated to have zero mean as well. In all the conducted experiments the patch size is set to five; thus the mask-patch has a dimensional size of 25 ($n=5 \times 5$). Our main rationale behind this selection is to keep the complexity of the local manifold of patches reasonably low. This is because sparse codes of data lying on smoother and more uniform manifolds tend to create more evenly distributed coefficients along the codebook's elements. Such cases are less prone to the phenomenon where very few dictionary elements are over-represented in the resulting sparse codes and are responsible for a significant amount of the total energy. Thus, they predominantly shape the distance between global image descriptors formed by these codes and require special pooling strategies to restore the discriminative power [36].

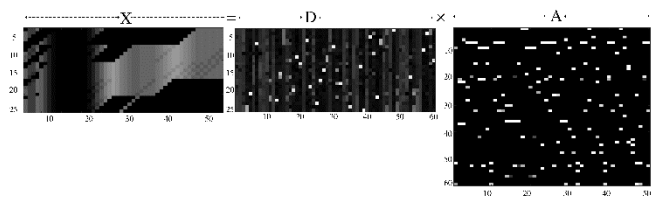


Fig. 5. Graphical illustration for signature coding with the use of SR. In this example, the matrix X consists of fifty 25-dimensional column-wise patches X^i of associated signature pixels. The lexicon D , consists of sixty atoms and is previously learned via a dictionary learning algorithm. The patch matrix X is represented as a linear combination of elements from D , with sparse coefficients given by A . Notice the sparse nature of A with few lines activated (appeared as

TABLE 1
OPERATIONAL PARAMETERS FOR SR METHODS

Process	Parameter	symbol	Value
<i>Thinning</i>	patch size	-	5
<i>K-SVD / OMP</i>	# maximum iterations	t_{\max}	50
	# atoms	K	60
	Sparsity level	ρ	3
<i>Online / LARS-Lasso</i>	mini-batch size	η	512
	# atoms	K	60
	regularization parameter	λ	0.15

With this aim, it is valuable to consider the parameters which affect the dimensionality and shape of the underlying local manifolds. In [37] Peyré shows that the local manifold of patches from cartoon images (images that contain sharp variations along regular curves) can be parameterized by two variables, leading to a manifold topologically equivalent to the surface of a cylinder in 3D space. This parameterization holds as long as the signal within each patch can be approximated by two regions (black and white) separated by a linear segment. If the patch size become larger and the edges within the patches appear curved, extra degrees of freedom have to be included to the signal's model thus leading to a more complex manifold. Similarly to cartoon images, the nature of the signal within signature patches is such that can be modeled by a handful of parameters if the patch size is small-enough, indicating a low-dimensional underlying manifold structure. On the other hand, the complexity can be dramatically increased if the patch size becomes large enough to contain curves and parts from neighboring line segments. We set patch size equal to 5, since it is a good tradeoff between the underlying signal's complexity since for smaller patches the local manifold obviously becomes degenerate - and the overall computational complexity. The later is dictated by the dictionary size whose over-completeness requirement points back to the patch dimensionality as the most significant parameter. It is worth noting that this scale of patches has also proven to be efficient in previous research efforts [7] on the particular problem, delivering state-of-the-art results and strengthening our decision on this selection.

3.3. SR-driven local feature extraction

Sparse Coding (SR) and consequent Dictionary Learning is a popular technique for handling computer vision problems. In this work, SR is involved in order to construct the dictionary (or \mathbf{D} for simplicity) that represents the characteristic properties of the signatory. The patches extracted from one signature are represented as columns of the matrix $\mathbf{X} \in \mathbb{R}^{n \times M}$ and the dictionary for sparse representation is updated via an iterative process, in which the patches of one reference signature are used in each update and ultimately, all the reference signatures are utilized in a cascade fashion. Hence, dictionary is updated consecutively using each one of the writer's genuine reference signatures. Thus, the system can integrate easily a new reference genuine signature of the writer and thus, it

is practical for application in everyday scenarios. Following the construction of the dictionary, for any other inserted signature image its patches are extracted and encoded using the dictionary and SR coding in order to obtain the sparse representation matrix \mathbf{A} . Figure 5 presents the SR concept as it is applied in the proposed method for signature modeling. Depending on the case, the dictionary learning and the sparse coding stages are implemented with either the K-SVD/OMP or the SPAMS/LARS-Lasso algorithm pairs. In addition, the impact on the system performance of some other popular optimization constraints is also explored with priors such as the positivity constraint of the coefficients, the non-negativity constraint for the dictionary atoms and the non-negative matrix factorization (NMF) method in which the matrix \mathbf{D} and the vectors \mathbf{A} are required to be positive. For the cases in which \mathbf{D} is positive, the SPAMS/LARS-Lasso algorithm is invoked but without the centering procedure of patches. It must be stated here that the centering procedure has not been applied for the case of having positive dictionary atoms and the NMF.

The operating parameters of the KSVD/OMP and the online/LARS-Lasso algorithms are summarized in Table 1. Specifically, for the KSVD/OMP case, the number of maximum iterations t_{\max} is set to fifty, as this number has been found experimentally that is adequate for all cases. The number of atoms K was set to sixty in order to ensure the over-completeness of the dictionary, which follows the rule of thumb that suggests a number of atoms more than twice the dimension of the patch size ([38], pg. 33). The sparsity level ρ is set to three in order to provide an overall of 5% sparsity on the coefficients given the fact that when ρ is small enough relative to K , the approximating methods are known to perform very well [39]. For the online/LARS-Lasso case, we use the same number of atoms K as in the KSVD/OMP case, while the number of signals drawn at each iteration or mini-batch size η , is set to 512, in order to improve the efficiency of the online dictionary learning algorithm ([38], pg.168). The dictionary learning algorithm is allowed to run for a typical execution time of one minute, which is considered adequate given the size of the signature patches. In addition, the regularization parameter λ is set to 0.15, a value which is in proximity to the classical $1/\sqrt{n}$ normalization factor proposed by Bickel et al. [40].

These parameters are a-priori fixed for all datasets and signatories and are not defined or tuned with neither a validation or test set. We should notice that we do not tune these parameters with a test set. In addition, we experimentally found that it is almost useless to consider a validation set, consisted of genuine and random forgeries, in order to optimize further any of the aforementioned parameters. That would make sense only in case where skilled forgeries are employed; however this protocol, in the WD training context, is usually not followed.

3.4. Pooling Strategies

It is common for contemporary computer vision algorithms to incorporate a pooling stage, which aggregates local features over a region of interest [41-43]. In this

work, a number of variants are proposed as signature descriptors by global aggregation of the local patch sparse coding coefficients into a final vector, through an appropriate pooling function. Depending on the pooling function, the corresponding signature descriptor is denoted hereafter as $f_I^{F1} - f_I^{F5}$, and defined as follows:

$$(F_1): f_I^{F1} = \{f_I^{F1}[j]\} = \left\{ \frac{1}{M} \sum_{i=1}^M \alpha^i[j] \right\}, j=1:K \quad (1)$$

$$(F_2): f_I^{F2} = \{f_I^{F2}[j]\} = \max(\alpha^i[j]), i=1:M, j=1:K \quad (2)$$

$$(F_3): f_I^{F3} = \{f_I^{F3}[j]\} = \left\{ \sqrt{\frac{\sum_{i=1}^M (\alpha^i[j] - f_I^{F1}[j])^2}{M-1}} \right\}, j=1:K \quad (3)$$

$$(F_4): f_I^{F4} = \{f_I^{F4}[j]\} = \frac{\sum_{i=1}^M \alpha^i[j]}{\sum_{j=1}^K \sum_{i=1}^M \alpha^i[j]}, j=1:K \quad (4)$$

$$(F_5): f_I^{F5} = \{f_I^{F5}[j]\} = \frac{\sum_{i=1}^M \alpha^i[j]}{\sqrt{\sum_{j=1}^K \left(\sum_{i=1}^M \alpha^i[j] \right)^2}}, j=1:K \quad (5)$$

Average pooling (F₁) is the simplest pooling function that estimates the average SR coefficients from the whole region of interest. The max pooling (F₂) operation only captures the most salient representation value from the entire region of interest. Standard deviation (F₃) is proposed here as an alternative pooling function that captures 2nd order statistics of the coefficients' distribution, in an aim to investigate if this type of information can deliver better discrimination capabilities to the resulting descriptor. Normalized Sum pooling (F₄) function produces vectors with intensity invariance, and finally the (F₅) function produces l^2 normalized vectors projected onto the unitary ball, which can be important for linear classification kernels [41].

The final feature vector's dimensionality provided by the preceding pooling operations is a multiple of the number of dictionary atoms K. In order to encapsulate local signature information to the final feature vector, a specially designed spatial pyramid is employed for segmenting the signature images into a grid of $(\beta \times \beta)$ equimass sub-regions. For each $I_{\beta}(t), t=1:\beta^2$ segment of this pyramid, its selected $\mathbf{x}_{I_{\beta}(t)}$ patches are enabled for indexing the local $\alpha_{I_{\beta}(t)}$ representation coefficients, which in their turn are subjected to the same pooling operations $F(\mathbf{A}_{I_{\beta}(t)})$ that is used for the computation of the $f_I^{F1} - f_I^{F5}$ global versions. As an aftermath, the dimensionality of the expanded feature $f^{Fg} = \{f_I^{Fg}, f_{I_{\beta}(t)}^{Fg}\}, g=1:5$, now equals to $(\beta^2 + 1) \times K$. In this work we tested the system's performance for two values of the β parameters, i.e. 2×2 and 3×3 equimass sub-regions for the spatial pyramid.

3.5. Emphasizing on informative local keypoints

A human expert, who wishes to analyze a signature image in order to verify if it is genuine or forgery, focuses on certain points of the signature. In an effort to discover these signature's points of interest we utilize the saliency-modeling mechanism implemented by the Binary Robust

Invariant Scalable Keypoints (BRISK) [34]. BRISK have the advantage of dramatically lowering computational complexity and thus are suited for low power devices, such as practical portable SV systems. BRISK computation relies on an easily configurable circular sampling pattern from which it computes brightness comparisons to form a binary 512 bit descriptor string and estimates keypoint scale in continuous scale-space. In this work only the detected keypoint locations and not the keypoint descriptors (BRISK) are utilized. Hence, keypoints indicate the patches, and thereafter the corresponding sparse codes will be once more pooled together in order to obtain an additional feature vector. This vector is concatenated with the spatial pyramid vector resulting to a final feature vector $f^{Fg} = \{f_I^{Fg}, f_{I_{\beta^2(1)}}^{Fg}, f_{I_{\beta^2(2)}}^{Fg}, \dots, f_{I_{\beta^2(\beta^2)}}^{Fg}\}$ of dimensionality is $(\beta^2 + 2) \times K$. Figure 6 depicts a zoomed area of an example signature image where the BRISK keypoints and their nearest signature pixels are denoted as crosses and x-points, respectively.

We provide a visualization, of the way that the signatures are distributed in the feature space by employing the t-SNE algorithm [44], [29] in order to map the genuine references, remaining genuine, skilled forgeries and random forgery samples from the initial R^{300} dimensional space to the projected R^2 space. Figure 7, displays the aforementioned information for F₃ type of feature, for one user and for the GPDS dataset.

4. EVALUATION

The selected classifier is a binary radial basis SVM classifier. In the learning stage of the classifier, each one of the N_{G-REF} genuine reference samples is encoded with the OMP or the LARS-Lasso SR algorithms in order to provide the positive class $\omega^+ \in R^{N_{G-REF} \times (Dim)}$ for each one of the feature $f_I^{F1} - f_I^{F5}$ descriptor given in (1)-(5). The negative training class $\omega^- \in R^{2 \times N_{G-REF} \times (Dim)}$ is composed by

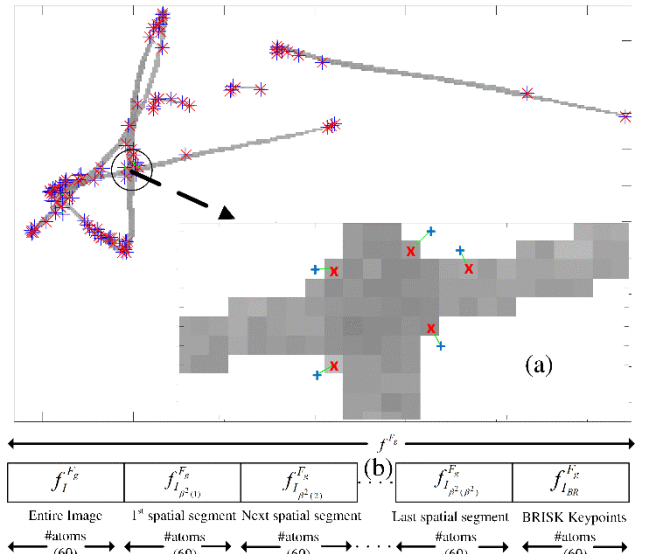


Fig. 6. a) Detail of a signature with BRISK keypoints. In the detail image, the marker (+) indicates the BRISK actual coordinates while (x) mark the assigned nearest signature pixel neighbors. b) Configuration of the various f^{Fg} in the overall feature vector. In this example, the number of atoms has been set to 60.

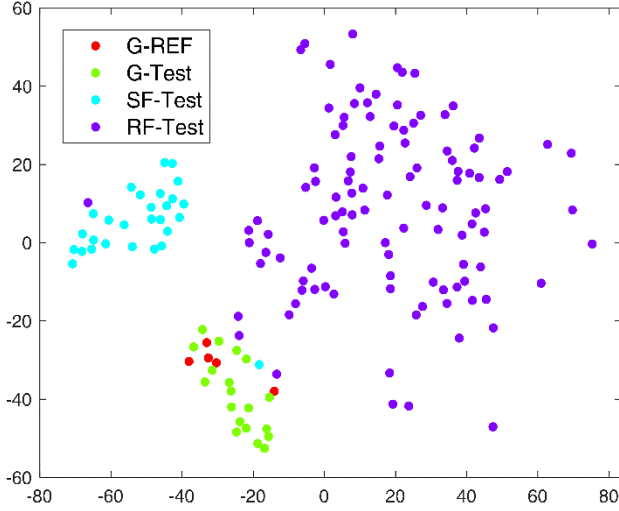


Fig. 7. t-SNE projection of the embedding space for the genuine reference (G-REF), remaining genuine (G-Test), skilled forgeries (SF-Test) and some random forgery samples (RF-Test) for F_3 feature type.

taking $2 \times N_{G-REF}$ random forgery samples; that is one genuine sample from a population of $2 \times N_{G-REF}$ writers different than the examined one. The learning feature set population $[\omega^+; \omega^-]$ is partitioned during the training / cross-validation procedure into a corresponding training and holdout validation set which serves as an input to the classifier. The holdout cross-validation procedure returns the optimal values of the C^{opt} and gamma- γ^{opt} parameters with respect to a maximum cross validation value of the associated Area Under Curve [45]. In addition, the cross-validation procedure stores the corresponding output scores CVS^{\oplus} which are conditioned upon the positive ω^+ class samples. The testing stage utilizes the remaining genuine samples, the skilled forgeries along with a number of random forgeries.

4.1. Datasets and Experimental Protocols

Four signature datasets are used in order to test the proposed system architecture. The first one is the popular CEDAR dataset [46]. For each one of the 55 enrolled writers, a total of 48 signature specimens (24 genuine and 24 simulated) confined in a 50 mm by 50 mm square box are provided and digitized at 300 dpi. The simulated signatures found in the CEDAR dataset are composed from a mixture of random, simple and skilled forgeries. The second signature dataset is the off-line version of the popular MCYT signature database [47, 48]. A whole of 30 signature samples (15 genuine and 15 simulated) signature samples are recorded for each one of the 75 enrolled writers at a resolution of 600 dpi and for and the capture area is 127×97 mm. Both CEDAR and MCYT-75 datasets have their samples confined within one bounding box. The third signature dataset is the GPDS300 [48, 49] which contains 24 genuine signatures and 30 simulated forgeries of 300 individuals stored in an 8-bit, grey level format. A special feature of this dataset is that the acquisition of signature specimens is carried out with the aid of two different bounding boxes of size 5×1.8 cm and 4.5×2.5 cm respectively. As a result, the files of this dataset include images having two different aspect ratios; this phe-

nomenon conveys a structural distortion highlighted during the feature extraction procedure. The fourth signature dataset is the Persian UTSIG, created by Soleimani et al. [50]. It contains specimens from 115 writers where each one has 27 genuine signatures, 3 opposite-hand signatures, and 42 skilled forgeries made by 6 forgers. As stated by the dataset creators, a property of the UTSIG dataset, compared with the other public and popular ones, is that UTSIG has more samples, more classes, and more forgers. An important characteristic of the UTSIG is that the acquisition of signature specimens is carried out with the aid of six different bounding box sizes simulating real world conditions and public services application forms. Since this work addresses writer depended signature verification, for any signatory a specific model is created by randomly employing N_{G-REF} genuine reference signature samples. The number of N_{G-REF} is primarily set to 5 for addressing cases in which only a few samples are available. In order to provide comparable results with other state-of-the-art methods, we allowed the N_{G-REF} parameter to assume values from 5 and/or 12 according to the specific needs of each dataset. The remaining genuine samples of a writer, as well as its forgeries and other writers' genuine samples have been used in order to form the test set.

A number of methods exist in order to quantify the efficiency of the proposed system. The false acceptance rate FAR and its associate probability P_{FAR} depicts a system's measure of the resistance to input samples other than the genuine ones like random or skilled forgeries. On the other hand, the FRR - false rejection rate and its accompanied probability rate P_{FRR} provides a system's measure of the failure to genuine samples. These operating system parameters are computed as a function of a sliding threshold whose extremes are located between the minimum and maximum values of the cross-validation SVM output scores CVS^{\oplus} . Some examples include independent experiments and corresponding solutions like: a) the P_{FAR}^S vs. P_{FRR}^S , where the upper script S denotes skilled forgery, along with their average AVE^S or equal error rates:

TABLE 2
VERIFICATION ERROR RATES (%) FOR THE CEDAR AND MCYT-75 SIGNATURE DATASETS WITH L_0 -NORM: KSVD/OMP DICTIONARY/SR METHODS. NUMBER OF REFERENCE TRAINING SAMPLES EQUALS 5. THE EER^S RATE CORRESPONDS TO THE USER SPECIFIC THRESHOLD CASE.

SET	F(A)	SP: $\beta = 2$ (Dim=360)				SP: $\beta = 3$ (Dim=660)			
		P_{FAR}^S	P_{FRR}^S	EER^S	$P_{FAR}^{R@FRR^S}$	P_{FAR}^S	P_{FRR}^S	EER^S	$P_{FAR}^{R@FRR^S}$
CEDAR	F1	6.83	7.32	2.67	0.43	6.13	7.18	2.80	0.27
	F2	9.45	9.83	4.17	2.93	8.83	8.65	3.21	0.76
	F3	4.76	4.91	1.44	0.17	4.78	5.63	1.80	0.12
	F4	8.12	9.94	7.51	1.95	12.7	20.2	13.4	4.82
	F5	5.31	5.27	3.08	0.35	5.05	5.11	2.48	0.24
MCYT-75	F1	10.4	7.32	3.80	0.22	9.18	7.12	3.19	0.14
	F2	14.7	14.6	10.9	3.16	15.6	11.5	8.65	1.12
	F3	8.09	6.75	3.18	0.16	8.07	6.21	2.82	0.07
	F4	12.99	16.17	10.8	3.08	11.0	23.7	16.7	6.17
	F5	7.64	7.76	3.23	0.14	7.77	7.92	3.46	0.13

TABLE 3
VERIFICATION ERROR RATES (%) FOR THE CEDAR AND MCYT-75 DATASETS WITH L_1 -NORM: PARAMETERS AS IN TABLE 1.

SET	F(A)	SP: $\beta = 2$ (Dim=360)				SP: $\beta = 3$ (Dim=660)			
		P_{FAR}^S	P_{FRR}	EER^S	$P_{FAR}^{R@EER^S}$	P_{FAR}^S	P_{FRR}	EER^S	$P_{FAR}^{R@EER^S}$
CEDAR	F1	6.99	7.60	2.65	0.37	6.59	6.61	3.08	0.23
	F2	9.42	9.71	3.45	1.55	8.52	8.01	2.80	0.48
	F3	4.61	4.64	1.62	0.12	4.88	5.81	2.01	0.08
	F4	8.19	8.73	3.52	0.56	9.17	8.71	3.97	0.41
	F5	7.05	7.81	3.38	0.41	5.49	6.48	3.07	0.22
MCYT-75	F1	10.46	8.57	3.91	0.24	7.82	7.68	3.58	0.14
	F2	15.8	14.3	11.20	3.09	13.9	12.3	8.60	1.08
	F3	8.35	7.58	3.71	0.22	7.59	7.29	3.40	0.10
	F4	12.2	13.43	3.93	0.30	9.82	9.68	3.53	0.15
	F5	7.87	7.59	3.66	0.20	7.07	7.69	3.05	0.12

$EER^S : P_{FAR}^S = P_{FRR}$, and b) the P_{FAR}^R vs. P_{FRR} , where the upper script R denotes random forgery, along with their corresponding average AVE^R or equal error rates $EER^R : P_{FAR}^R = P_{FRR}$. Other proposals provide joint solutions [51], which initially evaluate the $TH^{@EER^S}$ - threshold, defined as the value which designates the EER^S operating point and then, taking into account this value in order to assess the $P_{FAR}^{R@EER^S}$ error rate.

Regarding the choice of metrics, several researchers suggest handling SV as either a one class pattern recognition problem or a two class pattern recognition problem. The issue arises from the fact that the negative class of the test set has representatives from both skilled and random forgery samples [52]. The key point is that the skilled forgery class is composed of few samples compared with the random class. So, if one tries to incorporate both forgery populations there is always the danger of reporting biased results. For example, reporting an EER point of $EER^{R\&S} : \{P_{FAR}^{R\&S}\} = P_{FRR}$ where all types of forgery samples are employed; this is clearly biased since the forgery class has samples with two different populations of forgery. In this paper, as in [19, 20] the $EER_{user-threshold}^S$ is used by employing user-specific decision thresholds in order to evaluate the verification performance of the proposed system.

TABLE 5
VERIFICATION ERROR RATES (%) FOR THE GPDS300 AND UTSIG SIGNATURE DATASET WITH L_0 -NORM: NUMBER OF TRAINING SAMPLES EQUALS 5 AND [5, 12] FOR THE GPDS AND UTSIG.

SET	F(A)	SP: $\beta = 2$ (Dim=360)				SP: $\beta = 3$ (Dim=660)			
		P_{FAR}^S	P_{FRR}	EER^S	$P_{FAR}^{R@EER^S}$	P_{FAR}^S	P_{FRR}	EER^S	$P_{FAR}^{R@EER^S}$
GPDS300	F1	6.91	6.22	2.47	0.59	6.46	6.47	3.14	0.44
	F2	8.27	8.89	3.98	3.70	11.79	9.37	4.43	1.82
	F3	6.73	6.13	1.50	0.33	5.01	5.92	1.97	0.19
	F4	16.1	19.3	15.2	6.23	18.6	29.4	20.4	10.0
	F5	7.79	7.96	3.30	0.55	7.58	6.83	3.53	0.30
UTSIG-5G	F1	18.3	16.9	11.7	1.91	16.9	12.4	9.82	1.94
	F2	25.3	21.6	17.0	7.02	23.6	15.7	13.35	3.33
	F3	16.1	13.4	9.94	1.27	15.8	12.5	8.56	1.25
	F4	24.5	27.6	21.1	6.39	29.8	29.5	25.15	12.5
	F5	20.7	24.6	12.2	1.48	17.3	15.2	10.48	0.92
UTSIG-12G	F1	13.6	13.5	8.13	0.53	12.1	9.37	7.33	0.25
	F2	19.9	18.1	12.0	3.66	18.9	12.3	11.4	0.87
	F3	13.2	11.5	7.36	0.33	9.77	8.17	6.22	0.12
	F4	23.8	24.6	17.3	3.32	29.3	21.1	20.1	6.63
	F5	13.9	12.7	8.51	0.39	10.1	9.55	7.44	0.21

Also the calculation of the P_{FAR}^S, P_{FRR} rates with the utilization of a predetermined threshold (i.e. hard decisions) is provided by using the a-priori knowledge of the cross validation procedure scores CVS^\oplus . Specifically, the hard threshold value corresponds to the 50% of the average of the genuine CVS^\oplus scores for each writer. For completeness, at this specific threshold point the P_{FAR}^R error rate is evaluated by employing the genuine samples of the remaining writers from the test set.

5. EXPERIMENTAL RESULTS

For the sake of sanity and in order to avoid exhausting tests on all datasets, complete results are provided in tables 2-3 which involve the popular CEDAR and MCYT-75 datasets. All the experimental protocols are repeated ten times and the results are averaged in order to provide meaningful comparisons. It can be noticed that the verification error rates for the CEDAR and MCYT datasets do not vary substantially when both l_0 and l_1 -norms dictionary learning and SR are used. This is in accordance to the material exposed in Appendices A and B as well as in Section 3.3 which states that for a given dictionary \mathbf{D} both l_0 and l_1 oriented SR solutions are equivalent, for some specific values of the design parameters ρ and λ . Of course, the problem of locating the appropriate value for these design parameters is not a trivial one since it depends on the individual signature characteristics. An additional issue that arises is that tuning the system to a specific value either for ρ or λ depends mainly upon the different training modes. Moreover, we observed during the conducted experiments that the cross validation procedure, which is used for the selection of the optimal classifier parameters, is almost ineffective against skilled forgeries. A potential solution could emerge by employing WI systems with skilled forgeries which are not assigned to any specific person during the training. However, this approach is out of the scope of the present work.

The experimental outcomes show that the best results for the CEDAR dataset are obtained with the use of a spatial pyramid with $\beta = 2$ while for the MCYT-75 the optimal results are obtained with the use of a spatial pyramid with $\beta = 3$. This is probably due to the fact that CEDAR signature specimens have been scanned with a resolution of 300dpi, while the MCYT-75 ones with a resolution of 600dpi, thus it is natural to expect that more pixels exist in the MCYT-75 segments. It should be noticed that, for the CEDAR dataset even when the spatial pyramid with $\beta = 2$ is used, there are a few patches in some segments, which profoundly did not provide any sort of discriminatory information, something that has not been encountered in the case of the MCYT-75.

An important result that arises from our experimental results is that the accuracy for the F_3 pooling function seems to outperform all other pooling functions in almost all cases. It is also interesting that although the F_2 feature performs quite well in other computer vision applications, this is not the case for signatures images. A possible explanation relies on the very nature of the signature images which are a particular class of image signals that

TABLE 4

VERIFICATION ERROR RATES (%) FOR THE CEDAR AND MCYT-75 SIGNATURE DATASET WITH L_1 -NORM: AND FOR THE FOLLOWING PRIORS A) POSITIVITY CONSTRAINT OF THE \mathbf{A} COEFFICIENTS, B) THE 'NON-NEGATIVE' \mathbf{C}' CONSTRAINT FOR THE DICTIONARY ATOMS AND C) THE NMF METHOD. $\beta_{CEDAR} = 2$, $\beta_{MCYT} = 3$.

SET	F(A)	A positive				C' dictionary constrains				NMF			
		P_{FAR}^S	P_{IRR}	FFR ^s	$P_{FAR}^{R@EER^S}$	P_{FAR}^S	P_{IRR}	FFR ^s	$P_{FAR}^{R@EER^S}$	P_{FAR}^S	P_{IRR}	FFR ^s	$P_{FAR}^{R@EER^S}$
CEDAR	F1	7.26	7.99	2.38	0.29	7.29	7.72	2.43	0.34	9.13	8.41	2.22	0.39
	F2	9.56	9.07	3.19	1.52	9.32	9.84	3.63	1.72	22.5	24.2	16.3	13.3
	F3	4.74	4.92	1.77	0.15	4.97	4.96	1.71	0.26	6.48	9.41	1.52	1.09
	F4	10.3	9.69	3.91	0.45	10.3	9.94	3.00	0.45	12.7	10.3	3.05	1.04
	F5	9.98	7.69	3.17	0.35	9.83	9.99	2.78	0.32	9.78	9.36	2.64	0.54
MCYT-75	F1	12.6	8.96	4.71	0.31	11.1	10.6	5.53	0.44	10.2	10.9	4.34	0.45
	F2	19.4	18.3	12.4	3.43	18.8	19.4	11.9	2.50	30.8	30.4	24.3	20.3
	F3	12.2	8.44	4.97	0.22	10.9	9.67	4.86	0.33	13.4	12.9	7.99	1.78
	F4	14.4	11.3	5.38	0.59	13.6	14.1	5.34	0.45	17.2	18.1	6.69	1.98
	F5	11.3	10.2	4.69	0.35	11.4	10.2	4.97	0.27	11.8	1.6	4.48	0.37

exhibit a degenerate structure. Since all signature images essentially share a limited set of structural elements, the resulting sparse coefficients of different signatures may not differ sufficiently in a 1st order statistic sense, as being the case in more complex image structures. Therefore, it is reasonable to deduce that higher-order statistics can deliver a better level of discrimination between the respective distributions of sparse coefficients, resulting into better verification performance.

For further investigation we selected the spatial segmentation that corresponds to the best results, i.e. $\beta = 2$ for the CEDAR and $\beta = 3$ for the MCYT-75, and the l_1 -norm. Table 4 provides comparisons with exactly the same learning and testing samples for the following cases: a) the positivity constraint of the \mathbf{A} coefficients, b) the 'non-negative' \mathbf{C}' constraint for the dictionary atoms and c) the NMF method. The results indicate that none of these cases seems to provide any sort of significant improvement to the verification error. Thus, for the GPDS300 signature dataset and given the l_1/l_0 equivalence we will remain to the (l_0) norm expressed by the KSVD/OMP algorithms. Table 5, provides the corresponding results. As it is observed, F₃ still outperforms all other pooling functions. The increase of the spatial pyramid size from two to three does not provide any considerable verification improvement, except for the random forgery error as it is expressed from the P_{FAR}^R rate. We believe that this effect can be explained due to the indiscriminately nature of the spatial pyramid equimass segmentation which does not take into account the two different aspect ratios of the bounding box. As mentioned earlier, the UTSIG dataset is, according to the author's opinion, a significant realization step towards the assessment of situations which resemble typical conditions and constraints that are broadly encountered in daily transac-

tions. Table 5 also presents the results for our usual case of $N_{G-REF} = 5$. As expected, the provided verification results are poor regarding to the rates of the previous datasets however a closer look to P_{FAR}^R indicates that most likely the $N_{G-REF} = 5$ is not adequate in this case due to the large number of bounding box sizes. Therefore, in accordance with the literature [39], [9] and for comparison purposes, we let the value of N_{G-REF} raise up to twelve. Again, Table 5 presents the corresponding results. Table 5 provides evidence that the evaluation metrics rate drops significantly when the number of reference samples increases. Following and for the sake of simplicity, Table 6 shows comparative results by means of the $EER_{user-threshold}^S$ only for the case in which each input signature is thinned not by the MOTL value of the claimed writer's reference set but with an OTL number provided for each individual signature. Clearly, the results when using the MOTL value are inferior, an outcome that emphasizes the importance of the proposed preprocessing technique.

Table 7 demonstrates the influence of the segmentation profile to the verification performance in case of the CEDAR dataset. Specifically, the following five segmentation scenarios are examined a) using the entire image (EI), b) applying the SP segmentation, c) using only the BRISK keypoints, d) EI in conjunction with SP and finally e) a conjunction of EI, SP and BRISK keypoints. It is evident that the proposed segmentation approach that uses EI, SP and BRISK keypoints outperforms all the other scenarios for all pooling functions (with a minor exception of F₅). Moreover, F₃ pooling function, and corresponding feature vector persistently provides the best results in all segmentation scenarios and achieves the overall lower error in the proposed segmentation approach (last column of Table 6).

TABLE 6

INFLUENCE (EER %) OF THE VERIFICATION PERFORMANCE WHEN USING A) THE MOTL AND B) THE INDIVIDUAL OTL VALUES

F(A)	CEDAR		MCYT		GPDS300		UTSIG	
	MOTL	Ind.OTL	MOTL	Ind.OTL	MOTL	Ind.OTL	MOTL	Ind.OTL
F1	2.67	3.45	3.19	4.89	2.47	6.23	7.33	12.5
F2	4.17	5.20	8.65	10.2	3.98	8.65	11.4	24.9
F3	1.44	2.89	2.82	4.98	1.50	5.71	6.22	10.3
F4	7.51	9.42	16.7	20.5	15.2	20.5	20.1	26.0
F5	3.08	5.23	3.46	5.43	3.30	7.23	7.44	13.5

TABLE 7

INFLUENCE (EER %) OF THE VERIFICATION PERFORMANCE FOR DIFFERENT SEGMENTATION PROFILES OF THE CEDAR DATASET WITH L_0 -NORM: NUMBER OF REFERENCE SAMPLES IS 5

	Entire Image (EI)	SP: $\beta = 2$	BRISK only	EI & SP	EI & SP & BRISK
# Features	60	240	60	300	360
F1	8.87	4.10	8.35	2.78	2.67
F2	10.3	5.73	10.3	6.30	4.17
F3	4.36	2.98	4.30	1.95	1.44
F4	9.37	9.92	9.22	8.02	7.51
F5	8.20	4.38	8.47	3.04	3.08

TABLE 8

EFFECT OF NUMBER OF ATOMS (K) AND SPARSITY LEVEL (ρ) TO THE VERIFICATION ERROR (EER%).

	β	K=30		K=60			K=80		
		$\rho=1$	$\rho=3$	$\rho=1$	$\rho=3$	$\rho=6$	$\rho=1$	$\rho=4$	$\rho=8$
CEDAR	2	1.04	1.17	0.93	0.90	1.03	0.79	0.81	0.98
	3	1.31	1.51	0.98	1.14	1.52	0.91	1.04	1.32
MCYT	2	1.85	2.42	1.55	1.63	1.72	1.49	1.53	1.78
	3	1.98	2.26	1.55	1.97	1.95	1.37	1.58	1.73
GPDS-300	2	1.00	1.15	0.76	0.76	0.75	0.75	0.72	0.70
	3	1.07	1.20	0.93	0.92	0.92	0.90	0.85	0.86

In addition, we report a sensitivity analysis regarding the effect of the verification error that the dictionary learning and SR parameters have. Specifically, we run a set of experiments (KSVD/OMP only) with a variety of parameters: a) the number of dictionary atoms ($K=30$ or 60 or 80) and b) the number of sparsity level (1 or 3 for $K=30$, 1 or 3 or 6 for $K=60$ and 1 or 4 or 8 for $K=80$). The experiments resemble cases in which low, medium and high over-completed dictionaries are employed for $K=30$, 60 and 80 , respectively. Similar cases for high, medium and low sparsity levels were also taken into account. This time the experiments were conducted for CEDAR, MCYT and GPDS-300 datasets and with the use of 10 reference samples (12 for GPDS-300) in order to follow up with the most commonly encountered experimental setups in the literature. Table 8 presents the corresponding results. As a first comment on the results, it can be noticed that the use of a "low over-completeness" dictionary and corresponding SR provides lower verification error rates compared to the medium and high overcomplete dictionary /SR cases. Second, it seems that there is a correlation between lower verification error and the increasing number of dictionary atoms. Third, for the CEDAR and MCYT datasets, it is evident that a high sparsity level provides superior results compared to low or medium sparsity level. A possible explanation for this is that a higher order overcomplete dictionary creates and adapts more specific atoms to the learned structures while a higher sparsity level utilizes only the most dominant atom for the representation. This might mislead to the conclusion that a K-means algorithm should be followed instead. However, as stated in Section 2.1, the corresponding alpha coefficient of the most participating atom, during the SR process, is not one, as in the K-means case. Therefore our initial intuition for using SR seems to be justifiable. For the GPDS-300 more atoms are required to participate in order to low the verification error. The higher number of required atoms can be explained by the following facts: a) the GPDS-300 consists of thicker lines, thus more atoms are needed in order to represent a patch and b) GPDS signatures have been acquired with the use of two bounding boxes; so it is anticipated that more atoms should also participate in order to reconstruct the characteristic shapes that exist in a patch.

The performance of the proposed method has been tested also on degraded and noisy data. For this purpose, two different types of noise, namely Salt & Pepper, and Gaussian white noise were employed on the CEDAR dataset with various noise levels. It has been reported that

TABLE 9

RESULTS OBTAINED BY F_3 FEATURE AND WITH DIFFERENT TYPES OF NOISE FOR CEDAR DATASET.

Type of noise	Noise parameters			K=60			K=80		
	d	m	v	$\rho=1$	3	6	$\rho=1$	4	8
Salt & pepper	0.001	-	-	1.13	1.09	1.21	0.87	0.89	1.05
	0.01	-	-	1.01	1.03	1.15	0.88	0.90	1.07
	0.1	-	-	1.03	1.07	1.21	0.90	0.92	1.22
Gaussian	-	0	0.01	1.02	1.07	1.21	0.86	0.88	1.11
	-	0	0.1	2.94	2.94	2.98	2.86	2.91	3.21
	-	0.2	0.01	1.02	1.04	1.10	0.86	0.94	1.13

these two types of noise commonly appear in images during the data collection process [53]. Thus, we added noise in the original signature images as follows: a) Salt and Pepper with parameters $d=0.001$, 0.01 and 0.1 and b) Gaussian with mean and variance parameters i) $m=0$ & $v=0.01$, ii) $m=0$ & $v=0.1$ and iii) $m=0.2$ & $v=0.01$. Given that the images are now corrupted with noise we applied an additional typical preprocessing step with a median 3×3 filter for the case of Salt and Pepper noise. For the Gaussian noise case we also applied a denoising algorithm based on K-SVD which has been used in the literature [54]. The results are provided in Table 9. It can be noticed that the second order statistic feature (F_3) still outperforms any other type of feature. In addition, the overall performance of the proposed method remains relatively stable in the presence of noise. A closer insight reveals also that the part of the feature extraction method that is affected mostly from noise is the equimass segmentation and the corresponding spatial pyramid pooling.

As an additional comment on the results we could state that, as usual, the method does not perform well when the signatures of a signatory are either too simple or/and they present a significant amount of instability. This effect is quite strong in the case of using a limited number of reference samples (e.g. 5). Although the addition of more signature samples alleviates this effect, we report that this is still an open issue that a SV system must cope with. Perhaps a disadvantage of the used signature datasets so far is that there is not some additional information (e.g. the characterization by the signatories themselves of some of the genuine samples as outliers) which would allow us to tune better the learning stage of the classifier.

Perhaps the most challenging task on SV is the comparison of the results emanating from several state-of-the-art systems. This turns to become a difficult issue given the fact that, traditionally, the efficiency of SV's is evaluated under two independent scenarios: random forgeries and skilled forgeries. It has been reported [52] that while these scenarios are not necessarily unfitting, their use may lead to a misinterpretation of the results. Additionally, this kind of has been also stated to be unrealistic in typical real world cases [52]. Tables 10-12 outline and compare the $EER_{User_Threshold}^S$ based results of the proposed method, with emphasis to the F_3 pooling, to a number of state-of-the-art SV related methods regarding the four utilized datasets, on an EER or average error (AER) basis. The results clearly demonstrate that the proposed method achieves low verification errors that are at least comparable to the ones derived from other state-of-the-art meth-

ods. Having in mind the diversity of all other methods we comment that with respect to CEDAR, MCYT and UTSIG datasets, the reported error rate outperforms almost all other methods. Regarding to the GPDS case the reported results are also quite low, overpassed only by the method reported in [8] which is a DL oriented method.

6. CONCLUSIONS

In this paper the potential of Sparse Representation on creating discriminative features for accurate and efficient offline signature verification is presented. We thoroughly investigated the major aspects on the selection of the appropriate SR approach, and examined the effects of the associated parameters like the number of atoms, the sparsity level and the regularization function. We demonstrated that approximate greedy techniques can deploy the full potential of SR in a SV system, in a computationally attractive manner. We described a novel pooling scheme tailored to the problem of SV, and evinced that 2nd order statistics - standard deviation - can form more discriminative pooling functions in cases where signals exhibit degenerate structures. Finally, we proposed a carefully designed system, encompassing a novel algorithm for the automatic selection of the optimal thinning level, which is able to harness the power of SR in order to create a discriminative signature descriptor which obtains state-of-the-art results on the most challenging signature datasets. The method seems also to handle relative well noisy images that have undergone a typical preprocessing

TABLE 11
COMPARISONS WITH SV STATE-OF-THE-ART TECHNIQUES FOR MCYT-75 DATASET.

1st author Ref #	Method	# Ref.	AER / EER
Vargas [48]	L.B.P	5 / 10	11.9 / 7.08
Zois [7]	Partially Ordered Sets	5	6.02
Gilperez [67]	Contours	5 / 10	10.18 / 6.44
Alonso-Fernandez [68]	Slant and Envelope	5	22.4
Fierrez-Aguilar [69]	Global and Local Slant	10	9.28
Wen [70]	Invariant Ring Peripheral	5	15.0
Ooi [71]	Discrete Radon Transform	5 / 10	13.86 / 9.87
Soleimani [9]	HOG & Deep-MML	5 / 10	13.44 / 9.86
Hafemann [29]	SigNet / SigNet-F	10 / 10	2.87 / 3.00
Hafemann [8]	SigNet-SPP-300dpi	10	3.60
	SigNet-SPP-300dpi (finetuned)	10	2.33
Serdouk [14]	H.O.T	10	18.15
Okawa [43]	BoVW - VLAD - KAZE	10	6.4
Zois [20]	Archetypes	5	3.97
Zois [65]	Tree structured sparsity	5	3.52
Proposed	K-SVD/OMP (F₃)	10	1.37

denoising step.

TABLE 12
COMPARISONS WITH SV STATE-OF-THE-ART SV TECHNIQUES FOR GPDS AND UTSIG DATASETS.

TABLE 10
COMPARISONS WITH SV STATE-OF-THE-ART SV TECHNIQUES FOR CEDAR DATASET.

1st author Ref #	Method	# Ref.	AER / EER
Kumar R. [55]	Signature Morphology (WI)	1	11.6 / 11.8
Kumar R [56]	Surroundness (WI)	1	8.33
Kumar M. [57]	Chord moments	16	6.02
Chen [58]	Gradient+concavity	16	7.90
Chen [58]	Zernike moments	16	16.4
Kalera [46]	G. S & C (WI)	16	21.9
Zois [7]	Partially Ordered Sets	5	4.12
Guerbai [59]	Curvelet Transform (WI)	12	5.60
Serdouk [60]	Gradient LBP + LRF	16	3.52
Hafemann [29]	SigNet / SigNet-F	12 / 12	4.76 / 4.63
Hafemann [8]	SigNet-SPP-300dpi	10	3.60
	SigNet-SPP-300dpi (fine-tuned)	10	2.33
Bharathi [61]	Chain code	12	7.84
Okawa [12]	B.O.W with KAZE	16	1.60
Okawa [43]	V.L.A.D with KAZE	16	1.00
Ganapathi [62]	Gradient Direction	14	6.01
Shekar [63]	Morphological Pattern Spectrum	16	9.58
Hamadene [64]	Directional Co-occurrence (WI)	5	2.11
Zois [20]	Archetypes	5	2.07
Zois [65]	Tree structured sparsity	5	2.30
Dutta [13]	Compact Correlated Features	N/A	0.00
Tsourounis [66]	Deep Sparse Coding	5	2.82
Proposed	K-SVD/OMP	10	0.79

Dataset	1st author Ref #	Method	# Ref.	AER / EER
GPDS	Serdouk [60]	Gradient LBP + LRF	16	12.52
	Vargas [48]	L.B.P	12	6.20
	Favorskaya [72]	Global traits	15	12.72
	Bharathi [61]	Chain code	12	9.64
100	Ilu [73]	LBP & HOG & GLCM	10	7.66
160	Yilmaz [74]	HOG-LBP & SVM	12	6.97
	Nguyen [75]	MDF, Energy, Maxima	12	17.25
	Guerbai [59]	Curvelet Transform	8	15.95
	Ferrer [76]	Geometric Features	16	9.64
	Alaei [53]	LBP based	8 / 12	13.85 / 11.74
300	Zois [7]	Partially Ordered Sets	5	5.48
	Kumar R. [56]	Surroundness	1	13.76
	Eskander [77]	ESC-DPDF	12	17.82
	Soleimani [9]	HOG & Deep-MML	10	20.94
	Hafemann [29]	SigNet / SigNet-F	12 / 12	3.15 / 1.69
	Hafemann [8]	SigNet-SPP-300dpi	10	3.15
		SigNet-SPP-300dpi-F	10	0.41
	Parodi [78]	Circular Grid	13	4.21
	Serdouk [14]	H.O.T	10	8.76 / 9.30
	Pirlo [79]	Cosine similarity	12	7.20
	Pirlo [80]	Optical flow	6	4.60
	Hamadene [64]	Directional Co-occurrence	5	18.42
	Dutta [13]	Compact Correlated Features	N/A	11.21
960	Yilmaz [81]	Two channel CNN (WI)	12	2.05
		Two channel CNN & SigNet-F	12	0.88
300	Proposed	K-SVD/OMP (F₃)	12	0.70
UTSIG	Soleimani [9]	HOG-DMML	12	17.6
	Soleimani [50]	Fixed-point arithmetic	12	29.7
	Proposed	K-SVD/OMP (F₃)	12	6.22

Our future research plans include the exploitation of SR related techniques in order to construct a universal dictionary with the use of samples originating from a wide and diverse set of persons (instead of just only one signatory) in order to develop an efficient writer independent signature verifier.

REFERENCES

- [1] G. Pirlo, M. Diaz, M. A. Ferrer et al., "Early Diagnosis of Neurodegenerative Diseases by Handwritten Signature Analysis," *New Trends in Image Analysis and Processing -- ICIAP 2015 Workshops*, pp. 290-297.
- [2] L. G. Hafemann, R. Sabourin, and L. S. Oliveira, "Offline Handwritten Signature Verification - Literature Review," in 7th International Conference on Image Processing Theory, Tools and Applications (IPTA 2017), Montreal, Canada., 2017.
- [3] D. Impedovo, G. Pirlo, and R. Plamondon, "Handwritten Signature Verification: New Advancements and Open Issues," in *International Conference on Frontiers in Handwriting Recognition*, 2012, pp. 367-372.
- [4] R. Plamondon, G. Pirlo, and D. Impedovo, "Online Signature Verification," *Handbook of Document Image Processing and Recognition*, D. Doermann and K. Tombre, eds., pp. 917-947, London: Springer London, 2014.
- [5] S. Pal, M. Blumenstein, and U. Pal, "Off-line signature verification systems: a survey," in *Workshop on Emerging Trends in Technology*, Mumbai, Maharashtra, India, 2011, pp. 652-657.
- [6] Z. Zhang, K. Wang, and Y. Wang, "A Survey of On-line Signature Verification," in *Biometric Recognition*, Berlin, Heidelberg, 2011, pp. 141-149.
- [7] E. N. Zois, L. Alewijnse, and G. Economou, "Offline signature verification and quality characterization using poset-oriented grid features," *Pattern Recognition*, vol. 54, pp. 162-177, 2016.
- [8] L. G. Hafemann, L. S. Oliveira, and R. Sabourin, "Fixed-sized representation learning from offline handwritten signatures of different sizes," *International Journal on Document Analysis and Recognition (IJDAR)*, vol. 21, no. 3, pp. 219-232, September 01, 2018.
- [9] A. Soleimani, B. N. Araabi, and K. Fouladi, "Deep Multitask Metric Learning for Offline Signature Verification," *Pattern Recognition Letters*, vol. 80, pp. 84-90, 2016.
- [10] S. Dey, A. Dutta, J. I. Toledo et al., "SigNet: Convolutional Siamese Network for Writer Independent Offline Signature Verification," *arXiv preprint arXiv:1707.02131*, 2017.
- [11] M. Okawa, "Synergy of foreground-background images for feature extraction: Offline signature verification using Fisher vector with fused KAZE features," *Pattern Recognition*, vol. 79, pp. 480-489, 2018.
- [12] M. Okawa, "Offline Signature Verification Based on Bag-Of-Visual Words Model Using KAZE Features and Weighting Schemes," in *Proceedings of the IEEE Conference on Computer Vision and Pattern Recognition (CVPR) Workshops.*, 2016, pp. 184-190.
- [13] A. Dutta, U. Pal, and J. Lladós, "Compact correlated features for writer independent signature verification," in 2016 23rd International Conference on Pattern Recognition (ICPR), 2016, pp. 3422-3427.
- [14] Y. Serdouk, H. Nemmour, and Y. Chibani, "Handwritten signature verification using the quad-tree histogram of templates and a Support Vector-based artificial immune classification," *Image and Vision Computing*, vol. 66, no. Supplement C, pp. 26-35, 2017.
- [15] B. A. Olshausen, and D. J. Field, "Emergence of Simple-Cell Receptive-Field Properties by Learning a Sparse Code for Natural Images," *Nature*, vol. 381, no. 6583, pp. 607-609, 1996.
- [16] Z. Zhang, Y. Xu, J. Yang et al., "A Survey of Sparse Representation: Algorithms and Applications," *IEEE Access*, vol. 3, pp. 490-530, 2015.
- [17] J. Wright, Y. Ma, J. Mairal et al., "Sparse Representation for Computer Vision and Pattern Recognition," *Proceedings of the IEEE*, vol. 98, no. 6, pp. 1031-1044, 2010.
- [18] R. Rubinstein, A. M. Bruckstein, and M. Elad, "Dictionaries for Sparse Representation Modeling," *Proceedings of the IEEE*, vol. 98, no. 6, pp. 1045-1057, 2010.
- [19] E. N. Zois, I. Theodorakopoulos, D. Tsourounis et al., "Parsimonious Coding and Verification of Offline Handwritten Signatures," in 2017 IEEE Conference on Computer Vision and Pattern Recognition Workshops (CVPRW), 2017, pp. 636-645.
- [20] E. N. Zois, I. Theodorakopoulos, and G. Economou, "Offline Handwritten Signature Modeling and Verification Based on Archetypal Analysis," in 2017 IEEE International Conference on Computer Vision (ICCV), 2017, pp. 5515-5524.
- [21] S. Pal, A. Alireza, U. Pal et al., "Off-line Signature Identification Using Background and Foreground Information," in *International Conference on Digital Image Computing: Techniques and Applications*, 2011, pp. 672-677.
- [22] S. Pal, A. Alireza, U. Pal et al., "Multi-script off-line signature identification," in 12th International Conference on Hybrid Intelligent Systems (HIS), 2012, pp. 236-240.
- [23] B. Ribeiro, N. Lopes, and J. Gonçalves, "Signature identification via efficient feature selection and GPU-based SVM classifier," in *International Joint Conference on Neural Networks (IJCNN)*, 2014, pp. 1138-1145.
- [24] Khalajzadeh Hurieh, M. Mansouri, and M. Teshnehlab, "Persian Signature Verification using Convolutional Neural Networks," *International Journal of Engineering Research and Technology (IJERT)*, vol. 1, no. 2, pp. 7-12, 2012.
- [25] Z. Zhang, X. Liu, and Y. Cui, "Multi-phase Offline Signature Verification System Using Deep Convolutional Generative Adversarial Networks," in 2016 9th International Symposium on Computational Intelligence and Design (ISCID), 2016, pp. 103-107.
- [26] H. Rantzs, H. Yang, and C. Meinel, "Signature Embedding: Writer Independent Offline Signature Verification with Deep Metric Learning," in *International Symposium on Visual Computing*, Cham, 2016, pp. 616-625.
- [27] L. G. Hafemann, R. Sabourin, and L. S. Oliveira, "Writer-independent feature learning for Offline Signature Verification using Deep Convolutional Neural Networks," in 2016 International Joint Conference on Neural Networks (IJCNN), 2016, pp. 2576-2583.
- [28] L. G. Hafemann, R. Sabourin, and L. S. Oliveira, "Analyzing features learned for Offline Signature Verification using Deep CNNs," in 23rd International Conference on Pattern Recognition (ICPR), 2016, pp. 2989-2994.
- [29] L. G. Hafemann, R. Sabourin, and L. S. Oliveira, "Learning features for offline handwritten signature verification using deep convolutional neural networks," *Pattern Recognition*, vol. 70, pp. 163-176, 2017.

- [30] R. Kumar, B. Chanda, and J. D. Sharma, "A novel sparse model based forensic writer identification," *Pattern Recognition Letters*, vol. 35, pp. 105-112, 2014.
- [31] Y. Liu, Z. Yang, and L. Yang, "Online Signature Verification Based on DCT and Sparse Representation," *IEEE Transactions on Cybernetics*, vol. 45, no. 11, pp. 2498-2511, 2015.
- [32] L. Batista, E. Granger, and R. Sabourin, "Dynamic selection of generative-discriminative ensembles for off-line signature verification," *Pattern Recognition*, vol. 45, no. 4, pp. 1326-1340, 2012.
- [33] N. Andrew, and Y. Kai. "ECCV-2010 Tutorial: Feature Learning for Image Classification," ufldl.stanford.edu/eccv10-tutorial/.
- [34] S. Leutenegger, M. Chli, and R. Y. Siegwart, "BRISK: Binary Robust invariant scalable keypoints," in *International Conference on Computer Vision*, 2011, pp. 2548-2555.
- [35] N. Otsu, "A Threshold Selection Method from Gray-Level Histograms," *IEEE Transactions on Systems, Man and Cybernetics*, vol. 9, no. 1, pp. 62-66, 1979.
- [36] J. C. Yunchao Zhang, Xiuji Huang¹, Yongtian Wang, "A Probabilistic Analysis of Sparse Coded Feature Pooling and Its Application for Image Retrieval," *PLoS ONE*, vol. 10, no. 7, pp. 1-18, 2015.
- [37] G. Peyré, "Manifold models for signals and images," *Computer Vision and Image Understanding*, vol. 113, no. 2, pp. 249-260, 2009.
- [38] J. Mairal, F. Bach, and J. Ponce, "Sparse Modeling for Image and Vision Processing," *Found. Trends. Comput. Graph. Vis.*, vol. 8, no. 2-3, pp. 85-283, 2014.
- [39] M. Aharon, M. Elad, and A. Bruckstein, "K-SVD: An Algorithm for Designing Overcomplete Dictionaries for Sparse Representation," *IEEE Transactions on Signal Processing*, vol. 54, no. 11, pp. 4311-4322, 2006.
- [40] P. J. Bickel, Y. a. Ritov, and A. B. Tsybakov, "Simultaneous analysis of Lasso and Dantzig selector," *Ann. Statist.*, vol. 37, no. 4, pp. 1705-1732, 2009.
- [41] J. Feng, B. Ni, Q. Tian et al., "Geometric lp-norm feature pooling for image classification," in *CVPR 2011*, pp. 2609-2704.
- [42] H. Jégou, F. Perronnin, M. Douze et al., "Aggregating Local Image Descriptors into Compact Codes," *IEEE Transactions on Pattern Analysis and Machine Intelligence*, vol. 34, no. 9, pp. 1704-1716, 2012.
- [43] M. Okawa, "From BoVW to VLAD with KAZE features: Offline signature verification considering cognitive processes of forensic experts," *Pattern Recognition Letters*, vol. 113, pp. 75-82, 2018.
- [44] L. v. d. Maaten, and G. Hinton, "Visualizing data using t-SNE," *Journal of machine learning research*, vol. 9, pp. 2579-2605, 2008.
- [45] T. Fawcett, "An introduction to ROC analysis," *Pattern Recognition Letters*, vol. 27, no. 8, pp. 861-874, 2006.
- [46] M. K. Kalera, S. Srihari, and A. Xu, "Offline signature verification and identification using distance statistics," *International Journal of Pattern Recognition and Artificial Intelligence*, vol. 18, no. 07, pp. 1339-1360, 2004.
- [47] J. Ortega-Garcia, J. Fierrez-Aguilar, D. Simon et al., "MCYT baseline corpus: a bimodal biometric database," *IEE Proceedings Vision, Image and Signal Processing*, vol. 150, no. 6, pp. 395-401, 2003.
- [48] J. F. Vargas, M. A. Ferrer, C. M. Travieso et al., "Off-line signature verification based on grey level information using texture features," *Pattern Recognition*, vol. 44, no. 2, pp. 375-385, 2011.
- [49] M. Diaz, M. A. Ferrer, G. S. Eskander et al., "Generation of Duplicated Off-Line Signature Images for Verification Systems," *IEEE Transactions on Pattern Analysis and Machine Intelligence*, vol. 39, no. 5, pp. 951-964, 2017.
- [50] A. Soleimani, K. Fouladi, and B. N. Araabi, "UTSig: A Persian offline signature dataset," *IET Biometrics*, vol. 6, no. 1, pp. 1-8, 2016.
- [51] H. Loka, E. Zois, and G. Economou, "Long range correlation of preceded pixels relations and application to off-line signature verification," *IET Biometrics*, vol. 6, no. 2, pp. 70-78, 2016.
- [52] J. Galbally, M. Gomez-Barrero, and A. Ross, "Accuracy evaluation of handwritten signature verification: Rethinking the random-skilled forgeries dichotomy," in *IEEE International Joint Conference on Biometrics (IJCB)*, 2017, pp. 302-310.
- [53] A. Alaei, S. Pal, U. Pal et al., "An Efficient Signature Verification Method Based on an Interval Symbolic Representation and a Fuzzy Similarity Measure," *IEEE Transactions on Information Forensics and Security*, vol. 12, no. 10, pp. 2360-2372, 2017.
- [54] M. Elad, and M. Aharon, "Image Denoising Via Sparse and Redundant Representations Over Learned Dictionaries," *IEEE Transactions on Image Processing*, vol. 15, no. 12, pp. 3736-3745, 2006.
- [55] R. Kumar, L. Kundu, B. Chanda et al., "A writer-independent off-line signature verification system based on signature morphology," in *Proceedings of the 1st International Conference on Intelligent Interactive Technologies and Multimedia*, Allahabad, India, 2010, pp. 261-265.
- [56] R. Kumar, J. D. Sharma, and B. Chanda, "Writer-independent off-line signature verification using surroundedness feature," *Pattern Recognition Letters*, vol. 33, no. 3, pp. 301-308, 2012.
- [57] M. M. Kumar, and N. B. Puhan, "Off-line signature verification: upper and lower envelope shape analysis using chord moments," *IET Biometrics*, vol. 3, no. 4, pp. 347-354, 2014.
- [58] S. Chen, and S. Srihari, "A New Off-line Signature Verification Method based on Graph," in *Proceedings 18th International Conference on Pattern Recognition*, , 2006, pp. 869-872.
- [59] Y. Guerbai, Y. Chibani, and B. Hadjadji, "The effective use of the one-class SVM classifier for handwritten signature verification based on writer-independent parameters," *Pattern Recognition*, vol. 48, no. 1, pp. 103-113, 2015.
- [60] Y. Serdouk, H. Nemmour, and Y. Chibani, "New off-line Handwritten Signature Verification method based on Artificial Immune Recognition System," *Expert Systems with Applications*, vol. 51, pp. 186-194, 2016.
- [61] R. K. Bharathi, and B. H. Shekar, "Off-line signature verification based on chain code histogram and Support Vector Machine," in *International Conference on Advances in Computing, Communications and Informatics (ICACCI)*, 2013, pp. 2063-2068.
- [62] G. Ganapathi, and R. Nadarajan, "A Fuzzy Hybrid Framework for Offline Signature Verification," *5th International Conference on Pattern Recognition and Machine Intelligence*, P. Maji, A. Ghosh, M. N. Murty et al., eds., 2013, pp. 121-127, Berlin, Heidelberg.
- [63] B. H. Shekar, R. K. Bharathi, and B. Pilar, "Local Morphological Pattern Spectrum Based Approach for Off-line Signature Verification," *Pattern Recognition and Machine Intelligence: 5th International Conference on Pattern Recognition and Machine Intelligence*, P. Maji, A. Ghosh, M. N. Murty et al., eds., 2013, pp. 335-342, Berlin, Heidelberg.
- [64] A. Hamadene, and Y. Chibani, "One-Class Writer-Independent Offline Signature Verification Using Feature Dissimilarity

Thresholding," IEEE Transactions on Information Forensics and Security, vol. 11, no. 6, pp. 1226-1238, 2016.

[65] E. N. Zois, M. Papaggianopoulou, D. Tsourounis et al., "Hierarchical Dictionary Learning and Sparse Coding for Static Signature Verification," in 2018 IEEE Conference on Computer Vision and Pattern Recognition Workshops (CVPRW), 2018, pp. 432-442.

[66] D. Tsourounis, I. Theodorakopoulos, E. N. Zois et al., "Handwritten Signature Verification via Deep Sparse Coding Architecture," in 13th IEEE Image, Video, and Multidimensional Signal Processing Workshop (IVMSP), 2018, pp. 1-5.

[67] A. Gilperez, F. Alonso-Fernandez, S. Pecharroman et al., "Off-line Signature Verification Using Contour Features," in Proceedings 11th International Conference on Frontiers in Handwriting Recognition, Montreal, 2008.

[68] F. Alonso-Fernandez, M. C. Fairhurst, J. Fierrez et al., "Automatic Measures for Predicting Performance in Off-Line Signature," in IEEE International Conference on Image Processing, 2007, pp. 369-372.

[69] J. Fierrez-Aguilar, N. Alonso-Hermira, G. Moreno-Marquez et al., "An Off-line Signature Verification System Based on Fusion of Local and Global Information," Biometric Authentication, Lecture Notes in Computer Science D. Maltoni and A. K. Jain, eds., pp. 295-306: Springer Berlin Heidelberg, 2004.

[70] J. Wen, B. Fang, Y. Y. Tang et al., "Model-based signature verification with rotation invariant features," Pattern Recognition, vol. 42, no. 7, pp. 1458-1466, 2009.

[71] S. Y. Ooi, A. B. J. Teoh, Y. H. Pang et al., "Image-based handwritten signature verification using hybrid methods of discrete Radon transform, principal component analysis and probabilistic neural network," Applied Soft Computing, vol. 40, pp. 274-282, 2016.

[72] M. Favorskaya, and R. Baranov, "The off-line signature verification based on structural similarity," Frontiers in Artificial Intelligence and Applications, 2014, pp. 421-430.

[73] J. Hu, and Y. Chen, "Offline Signature Verification Using Real Adaboost Classifier Combination of Pseudo-dynamic Features", 12th International Conference on Document Analysis and Recognition, 2013, pp. 1345-1349.

[74] M. B. Yilmaz, and B. Yanikoğlu, "Score level fusion of classifiers in off-line signature verification," Information Fusion, vol. 32, Part B, pp. 109-119, 2016.

[75] V. Nguyen, M. Blumenstein, and G. Leedham, "Global Features for the Off-Line Signature Verification Problem," in 10th International Conference on Document Analysis and Recognition, 2009, pp. 1300-1304.

[76] M. A. Ferrer, J. B. Alonso, and C. M. Travieso, "Offline geometric parameters for automatic signature verification using fixed-point arithmetic," IEEE Transactions on Pattern Analysis and Machine Intelligence, vol. 27, no. 6, pp. 993-997, 2005.

[77] G. S. Eskander, R. Sabourin, and E. Granger, "Hybrid writer-independent writer-dependent offline signature verification system," IET Biometrics, vol. 2, no. 4, pp. 169-181, 2013.

[78] M. Parodi, J. C. Gomez, and A. Belaid, "A Circular Grid-Based Rotation Invariant Feature Extraction Approach for Off-line Signature Verification," 11th International Conference on Document Analysis and Recognition, 2011, pp. 1289-1293.

[79] G. Pirlo, and D. Impedovo, "Cosine similarity for analysis and verification of static signatures," IET Biometrics, vol. 2, no. 4, pp.

151-158, 2013.

[80] G. Pirlo, and D. Impedovo, "Verification of Static Signatures by Optical Flow Analysis," IEEE Transactions on Human-Machine Systems, vol. 43, no. 5, pp. 499-505, 2013.

[81] M. B. Yilmaz, and K. Ozturk, "Hybrid User-Independent and User-Dependent Offline Signature Verification With a Two-Channel CNN", IEEE Conference on Computer Vision and Pattern Recognition Workshops (CVPRW), 2018, pp. 526-534.



Elias N. Zois received his Bachelor's degree in Physics from the University of Patras (UoP), Patras, Greece (1994), the M.Sc. degree in Electronic Engineering from UoP (1996), along with his Ph.D. from UoP (2000). From 2000 to 2008, he has been working as an Adjunct Professor at the Technological and Educational Institute of Athens. Currently he is an Assistant Professor at the University of West Attica. His research interests include among other, computer vision, image processing, machine learning, and biometrics.



Dimitrios Tsourounis received his B.Sc. in Physics and M.Sc. in Electronics and Information Processing from the Physics Dept., University of Patras, Greece in 2015 and 2017. He is now a Ph.D. candidate in Machine Learning at the Physics Department of the University of Patras. His research interests include Machine Learning, Pattern Recognition, Image Processing, Computer Vision applications and Biometrics.



Ilias Theodorakopoulos received a B.Sc. degree in Physics in 2007, a M.Sc. degree in Electronics and Computers in 2009 and a Ph.D degree in Pattern Recognition & Manifold Learning in 2014, all from University of Patras. He works as a data scientist and researcher in the fields of Machine Learning and Data Analysis, having more than 20 publications and 3 patents (granted and pending). His research interests include theoretical foundations of Machine Learning, applications on Computer Vision, Biometric Identification and Biomedical Data Analysis.



Anastasios L. Kesidis received his B.S and Ph.D degrees in Electrical and Computer Engineering from Democritus University of Thrace, Xanthi, Greece, in 1995 and 2001, respectively. From 2000 to 2002 he worked as a postdoctoral Research Fellow in Centre for Vision, Speech and Signal Processing, University of Surrey, UK and from 2005 to 2010 he joined the National Centre for Scientific Research "Demokritos", Athens, Greece as a Research Scientist. Currently he is an

Associate Professor in the Department of Surveying and Geoinformatics Engineering at the University of West Attika, Greece. His research interests include image processing, pattern recognition and machine learning.



George Economou received his Bachelor's degree in Physics from the University of Patras (UoP), Patras, Greece (1976), the M.Sc. degree in Microwaves and Modern Optics from University College, London, U.K. (1978), and the Ph.D. degree in 'Fiber optic sensor systems' from UoP (1989). From 1983 to 1985, he has been working as a Visitor Research Assistant at University College London. He is currently Professor with the Department of Physics University of Patras. His research interests include computer vision, image processing, machine learning, pattern recognition and biometrics.

APPENDIX A – SPARSE CODING

Informally, the objective of Sparse Representation (SR) is to encode a set of signals as a linear combination of a few elements of a predefined set (dictionary) whose elements are defined as basis vectors or atoms. The sparse dictionary is usually overcomplete i.e. the number of dictionary elements is higher than the input signal's dimensions. Several techniques for SR have been successfully applied in the fields of computer vision, pattern recognition and machine learning. The key idea is to represent an observed phenomenon through the activation of only as few components as possible. It has been shown that the V_1 part of the brain which receives visual stimuli, is alleged to perform a similar process with sparsity objectives [1]. For an overcomplete dictionary $\mathbf{D} = [\mathbf{d}^1, \mathbf{d}^2, \dots, \mathbf{d}^K] \in \mathbb{R}^{n \times K}$ with $K > n$ and for M input signals $\mathbf{X} = [\mathbf{x}^1, \mathbf{x}^2, \dots, \mathbf{x}^M] \in \mathbb{R}^{n \times M}$, the formulation of SR is usually expressed with the following equivalent forms of regularized or constraint optimization problem expressed by (1) and (2) respectively:

$$\frac{1}{M} \sum_{i=1}^M \min_{\mathbf{a}^i} \left(\frac{1}{2} \|\mathbf{x}^i - \mathbf{D}\mathbf{a}^i\|_2^2 + \lambda \psi(\mathbf{a}^i) \right) \quad (1)$$

$$\frac{1}{M} \sum_{i=1}^M \min_{\mathbf{a}^i} \left(\frac{1}{2} \|\mathbf{x}^i - \mathbf{D}\mathbf{a}^i\|_2^2 \right), \text{ s.t: } \psi(\mathbf{a}^i) \leq \rho, \forall i=1:M \quad (2)$$

In the above expressions (1), (2), the matrix $\mathbf{A} = [\mathbf{a}^1, \mathbf{a}^2, \dots, \mathbf{a}^M] \in \mathbb{R}^{K \times M}$ represents the sparse coefficients for the M input signals, $\|\mathbf{x}^i - \mathbf{D}\mathbf{a}^i\|_2^2$ is the reconstruction error, λ is the regularizer parameter or Lagrange multiplier and $\psi(\bullet)$ is the sparsity-inducing term [2]. The embedded term $\psi(\bullet)$ is defined to be the l_p -norm (defined for $1 \leq p \leq \infty$) of the coefficients \mathbf{a}^i , i.e. $\psi(\mathbf{a}^i) = l_p(\mathbf{a}^i) = \|\mathbf{a}^i\|_p = \left(\sum_{j=1}^K (\mathbf{a}^i[j])^p \right)^{1/p}$ for a specific value of p . The most popular forms are the ones that rely on the l_0 -norm and l_1 -norm, i.e. for $p=0$ or $p=1$. Specifically, the l_0 -norm or pseudo-norm is equal to the count of non-zero elements ρ (sparsity level) of the representation vector \mathbf{a}^i and so it is the most direct sparsity measure. However, this selection leads to a combinatorial NP-hard optimization problem, whose solution can only be approximated [3]. On the contrary, the l_1 -norm leads into a convex relaxation of the coding problem and has been proved that encourages sparse solutions [3]. Thus, the sparsity inducing term is usually utilized by the l_0 -norm which is a greedy non-convex approximation and the l_1 -norm which is a convex relaxation named Lasso [4].

To obtain a satisfactory solution of Sparse Coding with the use of the l_0 -norm regularization term, greedy algorithms can be utilized in order to seek and provide an approximate optimized solution. The idea behind the greedy strategy is to always seek for the atom with the strongest relation to the sample under examination, in an effort to aggressively reduce the reconstruction error in the least-squares sense. The orthogonal matching pursuit (OMP) [5] along with a number of variations like regularized OMP, stage wise OMP, sparsity adaptive matching pursuit, are typical representatives of greedy algorithms. Given a dictionary \mathbf{D} and any sample \mathbf{x}^i , OMP sequentially selects the atoms with the highest correlation to the respective sample's residual. At a step $s: 0 < s \leq \rho$ the

selected atom is given by: $k_s = \arg \max_j |(\mathbf{d}^j)^T \mathbf{r}_{s-1}|$, where \mathbf{r}_{s-1} is the current residual. Once an atom is selected, the \mathbf{x}^i signal is projected onto the span of currently selected atoms as: $\hat{\mathbf{a}}_s = (\mathbf{D}_{V_s})^+ \mathbf{x}^i$, where $V_s = V_{s-1} \cup k_s$ is the set of indices pointing at the currently selected dictionary atoms, and \mathbf{D}_{V_s} is the subset of dictionary indexed by V_s . The new residual is now given by $\mathbf{r}_s = \mathbf{x} - \mathbf{D}_{V_s} \hat{\mathbf{a}}_s$ while the process now repeats until either ρ atoms are selected or the residual magnitude minimizes. In this work we utilized the batch-OMP implementation [6], which makes use of Cholesky decomposition in order to reduce the computational cost of repeated re-projections, as a means to assess the efficiency of greedy SR methods in signature verification.

The use of the l_1 -norm, has been also broadly proposed for sparse solutions since it provides an analytical solution and can be solved in polynomial time. Solvers for handling the l_1 -norm oriented SR problems, include the well-known basis pursuit [7] and the Lasso [4] among others. A number of methods for solving the l_1 -norm problems rely on coordinate descent methods, which have been found to be efficient enough in cases where dictionary atoms exhibit low correlation. Unlike, when the atoms of the dictionary are highly correlated, homotopy-based methods can be applied. The homotopy methods solve the regularized sparse coding optimization problem, as expressed by (1), and track the entire regularization path (i.e. the solutions for all possible values of λ), like the least angle regression (LARS-Lasso) algorithm [8]. The LARS-Lasso algorithm calculates the solution path by repeatedly decreasing the value of λ and using as a warm-restart of the previously calculated solution. The uniqueness of the solution for a specific value of the parameter λ , i.e. the existence of a single normalized path solution, is ensured and it can be proved that the solution path is piecewise linear [9]. This property is very important since the algorithm follows the direction of each segment until it reaches a critical point, i.e. where either a non-zero element becomes zero (so it is removed from the active set of coefficients) or a new non-zero element is added to the active set of coefficients. Therefore, the homotopy method initializes with an empty set of coefficients, and iteratively updates it by one variable at a time. The complexity of the method relies in reversing the covariance matrix of the selected atoms at each critical point in order to update the active set of coefficients, which is performed by the Cholesky decomposition or the Woodbury formula. In this work the LARS-Lasso algorithm, which is a part of the SPAMS toolbox [9], has been utilized to investigate the efficiency of sparse coding with convex relaxation.

APPENDIX B – DICTIONARY LEARNING

The most efficient way for dictionary construction is through a learning process that enables the dictionary (i.e. atoms) to be fitted to the input-training data. The most common dictionary learning methods are unsupervised and have been mainly utilized for image processing problems, such as image compression and super resolution.

Although these methods are not explicitly enforcing discriminative behavior to the sparse coefficients since the cost function relies only on reconstruction error, they have been used for classification tasks with remarkable results [10]. The sparse representation problem (i.e. dictionary learning and sparse coding) is a joint optimization problem with respect to dictionary \mathbf{D} as well as the coefficients $\mathbf{A} = \{\mathbf{a}^i\}$ and it is expressed as follows:

$$\min_{\mathbf{D} \in C, \mathbf{A} \in \mathbb{R}^{K \times M}} \left(\frac{1}{2} \|\mathbf{X} - \mathbf{D}\mathbf{A}\|_F^2 + \lambda \|\mathbf{a}^i\|_p \right) \quad (3)$$

$$\min_{\mathbf{D} \in C, \mathbf{A} \in \mathbb{R}^{K \times M}} \left(\frac{1}{2} \|\mathbf{X} - \mathbf{D}\mathbf{A}\|_F^2 \right) \text{ s.t.: } \|\mathbf{A}\|_p \leq \rho \quad (4)$$

where the set C of the dictionary atoms is usually defined to be the convex set of matrices that satisfy the following constraint: $C \triangleq \{\mathbf{D} \in \mathbb{R}^{n \times K} \text{ s.t.: } \forall_{j=1:M}, (\mathbf{d}^j)^T \mathbf{d}^j \leq 1\}$ in order to avoid large values, which consequently might lead to arbitrarily small values for the coefficients.

The greedy approximation of l_0 -norm regularized SR is addressed in this work by means of the KSVD [11, 12] and the associated OMP algorithm for dictionary learning and sparse coding respectively. For the convex relaxation approach, the online learning method [9] along with the LARS-Lasso algorithm have been employed for the corresponding tasks. In the case of the KSVD/OMP algorithm pair, the notation of eq. (4) has been selected due to the fact that the use of the l_0 sparsity constraint $\|\mathbf{A}\|_0 \leq \rho$ with $\rho \in \mathbb{N}^+$, intuitively assigns as a design parameter the integer number of the non-zero elements ρ . On the other hand, for the case of online/LARS-Lasso algorithm pair the notation of eq. (3) has been followed due to the fact that the interpretation of the parameter $\rho_1 \in \mathbb{R}$ in the ℓ_1 constraint $\|\mathbf{A}\|_1 \leq \rho_1$ does not provide any thoughtful intuition regarding the sparsity of the atoms as a design parameter. Instead, the parameter λ of eq. (3) shall be used as the design parameter of the method which now controls the sparsity. From a theoretical point of view, for an appropriate dictionary, the solution obtained with the use of the ℓ_1 -norm is equivalent to the one provided by another ℓ_0 -norm based solution with full probability [13, 14], [3]. However, this ℓ_1 / ℓ_0 equivalence phenomenon, does not hold in the case of the joint regularized and constrained dictionary learning problem since it has been reported that different formulations of the dictionary learning problem do not admit the same solutions even for the case of using the same ℓ_1 -norm [9]. That is the reason behind our decision to evaluate the performance of both ℓ_0 and ℓ_1 -norm approaches.

Access, vol. 3, pp. 490-530, 2015.

- [4] R. Tibshirani, "Regression Shrinkage and Selection via the Lasso," *Journal of the Royal Statistical Society. Series B (Methodological)*, vol. 58, no. 1, pp. 267-288, 1996.
- [5] J. A. Tropp, and A. C. Gilbert, "Signal Recovery From Random Measurements Via Orthogonal Matching Pursuit," *IEEE Transactions on Information Theory*, vol. 53, no. 12, pp. 4655-4666, 2007.
- [6] R. Rubinstein, M. Zibulevsky, and M. Elad, "Efficient implementation of the K-SVD algorithm using batch orthogonal matching pursuit," *CS Technion*, vol. 40, no. 8, pp. 1-15, 2008.
- [7] S. S. Chen, D. L. Donoho, and M. A. Saunders, "Atomic Decomposition by Basis Pursuit," *SIAM Review*, vol. 43, no. 1, pp. 129-159, 2001.
- [8] B. Efron, T. Hastie, I. Johnstone *et al.*, "Least angle regression," *Ann. Statist.*, vol. 32, no. 2, pp. 407-499, 2004/04, 2004.
- [9] J. Mairal, F. Bach, J. Ponce *et al.*, "Online Learning for Matrix Factorization and Sparse Coding," *J. Mach. Learn. Res.*, vol. 11, pp. 19-60, 2010.
- [10] J. Wang, J. Yang, K. Yu *et al.*, "Locality-constrained Linear Coding for image classification." pp. 3360-3367.
- [11] R. Rubinstein, A. M. Bruckstein, and M. Elad, "Dictionaries for Sparse Representation Modeling," *Proceedings of the IEEE*, vol. 98, no. 6, pp. 1045-1057, 2010.
- [12] M. Aharon, M. Elad, and A. Bruckstein, "K-SVD: An Algorithm for Designing Overcomplete Dictionaries for Sparse Representation," *IEEE Transactions on Signal Processing*, vol. 54, no. 11, pp. 4311-4322, 2006.
- [13] D. L. Donoho, "For most large underdetermined systems of linear equations the minimal " *Communications on Pure and Applied Mathematics*, vol. 59, no. 6, pp. 797-829, 2006.
- [14] D. L. Donoho, *Neighborly polytopes and sparse solution of underdetermined linear equations.*, Department of Statistics, Stanford University, 2004.

- [1] B. A. Olshausen, and D. J. Field, "Emergence of Simple-Cell Receptive-Field Properties by Learning a Sparse Code for Natural Images," *Nature*, vol. 381, no. 6583, pp. 607-609, 1996.
- [2] J. Yang, L. Zhang, Y. Xu *et al.*, "Beyond sparsity: The role of L1-optimizer in pattern classification," *Pattern Recognition*, vol. 45, no. 3, pp. 1104-1118, 2012/03/01/, 2012.
- [3] Z. Zhang, Y. Xu, J. Yang *et al.*, "A Survey of Sparse Representation: Algorithms and Applications," *IEEE*

Appendix C – Main Code - Pseudocode of the proposed method

Main Algorithm: Dictionary Learning and sparse coding of signature images
Require: The signatures of a dataset,
BEGIN
1: **SELECT:** One signatory (wrn) from the signature dataset.
2: **DEFINE: Learning SET** from the wrn -signatory
 $\{\omega^{\oplus}\}$: $\#N_{G-REF}$ Genuine Reference Samples, randomly selected (e.g. 5)
 $\{\omega^{-}\}$: $\#2 \times N_{G-REF}$ Genuine Samples from other signatories (e.g. 10)
 $PS = patch_size$ (e.g. 5); $PS^2: PS \times PS$
 p : number of dictionary atoms ($> 2 \times patch_size$, e.g. $p=60$),
3: **DEFINE: Testing Set** for the wrn -signatory
 Remaining Genuine Samples (e.g. 19 for CEDAR)
 All forgeries (e.g. 24 for CEDAR)
 Random forgeries (e.g. 54 for CEDAR)
4: **CALL ALGORITHM 1** and **DEFINE** MOTL for ω^{\oplus} samples
5: **FOR** $j = 1$ **UP TO** size of $\{\omega^{\oplus}\}$
6: **PREPROCESS:** Threshold, $thin_with_MOTL$ the signature image.
7: **EXTRACT** all patches $X \in \mathbb{R}^{PS^2 \times (\#patches)}$; **CENTER** each patch $X_k \in \mathbb{R}^{PS^2 \times 1}$
8: **IF** $j=1$ then
 USE Dictionary Learning algorithm (e.g. K-SVD). **RETURN** $D \in \mathbb{R}^{PS^2 \times p}$
ELSE
 UPDATE $D \in \mathbb{R}^{PS^2 \times p}$ with new patch matrix $X \in \mathbb{R}^{PS^2 \times (\#patches)}$
end_IF
9: **end_FOR**
10: **FOR** any signature of $\{\omega^{\oplus}, \omega^{-}, \text{Testing Set}\}$: **APPLY** steps 6, 7:
11. **USE** OMP or LASSO for evaluation of sparse coefficients $A \in \mathbb{R}^{p \times (\#patches)}$
12. **USE** some poolingFunction($A \in \mathbb{R}^{p \times (\#patches)}$), **CREATE** features $F \in \mathbb{R}^{p \times 1}$
13. **FOR** any other signature segment (Equimass, BRISK)
14. **REPEAT** steps 6, 7, **APPEND** and **UPDATE** F to $F \in \mathbb{R}^{[p \times (\#segments)] \times 1}$
15. **end_FOR**
16: **end_FOR.** % Features for all signatures
17: **TRAIN** and **CROSS_VALIDATE** with $\{\omega^{\oplus}, \omega^{-}\}$
18: **TEST** with **Testing Set**

Appendix D – OTL (and MOTL) Pseudocode

Algorithm 1: Define optimal thinning level.
Require: $B_i, i=1: N_{G-REF}$ Reference binary set of images, N_p - patch size.
1: **for** $i=1: N_{G-REF}$
 2: **set** th_lev **EQUAL TO** 0 % (thinning level)
 3: **Repeat**
 4: $TH_{th_lev}^i = \text{THIN_OPERATION}(B_i, th_lev)$
 5: **Create** map with locations of $TH_{th_lev}^i$ signature pixels.
 6: **for** j = each signature pixel of the map
 Impose a $N_p \times N_p$ patch, centered at the coordinates of the j -pixel.
 Measure the number of signature pixels that reside in the patch.
 Normalize by $N_p \times N_p$ and **ASSIGN** value to $LD(j)$.
 end for
 7: **Evaluate** mean value of LD and **ASSIGN** value to $PD(th_lev)$.
 8: $th_lev \leftarrow th_lev + 1$ (increase thinning level)
 9: **Until** $TH_{th_lev}^i = TH_{th_lev+1}^i$ (has idempotent stage reached?)
 10. **Find** minimum of the difference of the PD function,
 11. **RETURN** minimum index to **OTL(i)**.
12: **end for**
Return: MOTL: The median value of **OTL**.